Diamond & Related Materials xxx (xxxx) 111837

Contents lists available at ScienceDirect

Diamond & Related Materials

journal homepage: www.elsevier.com/locate/diamond

Formation and depth distribution of optically active centers in diamond implanted with high energy xenon ions

N.M. Kazuchits [a,*], V.N. Kazuchits [a], O.V. Korolik [a], M.S. Rusetsky [a], V.A. Skuratov [b,c,d], A.M. Zaitsev [e]

[a] Belarusian State University, Nezavisimosti av. 4, 220030 Minsk, Belarus
[b] Joint Institute for Nuclear Research, Joliot-Curie 6, 141980 Dubna, Russia
[c] National Research Nuclear University MEPhI, Moscow, Russia
[d] Dubna State University, Dubna, Russia
[e] College of Staten Island/CUNY, 2800 Victory Blvd., Staten Island, NY 10314, USA

ARTICLE INFO

Keywords:
Diamond
Ions implantation
Radiation damage
Raman scattering
Photoluminescence

ABSTRACT

The depth distributions of the spectral parameters of Raman and luminescence features of diamond implanted with Xe ions of an energy 167 MeV have been studied in as-irradiated state and after post-irradiation annealing. The Raman data show that the distribution of radiation defects in the as-irradiated layer follows the nuclear stopping power of the ions. It has been found that the two major mechanisms determining the distribution of intensity of the luminescence centers are the quenching due to crystal lattice damage and the instantaneous heating due to intense electronic stopping. It has been shown that the strong nuclear stopping at the end of the ion penetration produces a highly disordered buried layer. The atomic structure of this layer completely loses its crystallinity for ion fluences above 3×10^{14} cm^{-2}. This atomic structure does not collapse into graphite during high temperature annealing and can be regarded as amorphous diamond. It has been shown that the post-irradiation annealing produces secondary radiation defects far deeper than the depth of the ion penetration. This deep defect production is explained by the dislocations propagating from the disordered layer into the diamond bulk during heating.

1. Introduction

Diamond is one of the most suitable materials used for studies of the defects produced by high energy ion implantation. Diamond reveals strong Raman scattering which is very sensitive to the presence of non-diamond phases [1,2], and it has a number of highly efficient luminescence centers related to point radiation defects of different types [3]. These advantages become especially valuable when the Raman and luminescence of the ion-implanted diamond is studied using spectrometers with high spatial resolution. It allows us to obtain detailed information on the radiation defects formed in the areas with different contribution of the electronic and nuclear stopping, and on the evolution of the radiation damage during post-irradiation processing.

Structural effects of the electronic stopping during swift heavy ion irradiation are usually associated with strong local heating/melting in nanometric volume surrounding ion trajectory (for example, [4]). Since such temperature rise lasts for hundreds of picoseconds, its effect is not expected to be equivalent to the effect of stationary annealing typical duration of which is a few tens of minutes. However, since the peak temperature during ion stopping is very high, its action may result in measurable changes in the defect structure even if the heating time is very short. Diamond has many radiation optical centers the intensity of which changes at relatively low temperatures [5,6]. Thus, these centers might be used as indicators of heating occurring during ion-irradiation.

The average penetration depth (projected range) of heavy ions of an energy 1 MeV/amu in diamond is about 10 μm [7]. In the first few microns of the ion path the nuclear stopping is negligible, and the created radiation defects are few. As ions penetrate deeper the electronic stopping decreases while the nuclear stopping increases first gradually and then drastically at the end of the ion path. Synchronously with the nuclear stopping the concentration of the radiation defects increases too [8]. The increasing defect concentration causes swelling which reaches maximum at the depth of maximum nuclear stopping [9–12]. It is to point out that the electronic stopping, although inefficient in the direct

* Corresponding author.
E-mail address: kazuchits@bsu.by (N.M. Kazuchits).

https://doi.org/10.1016/j.diamond.2024.111837
Received 8 October 2024; Received in revised form 29 November 2024; Accepted 30 November 2024
0925-9635/

radiation damage when alone, may noticeably affect (stimulate, suppress, or alter) the defect production caused by the nuclear stopping [13].

In this research we studied the depth distribution of the radiation damage in diamond implanted with high energy Xe ions. The obtained results revealed a characteristic three-layer defect structure, which, we assume, is the general feature of high energy ion implantation.

2. Material and methods

Implantation with 167 MeV Xe ions (also referred as ion irradiation) was performed using cyclotron IC-100 FLNR of JINR institute (Dubna, Russia) with several fluences following the procedure described [7]. The samples were subjected to the range of ion fluences. Two fluences of 6.1×10^{12} cm^{-2} and 8.15×10^{14} cm^{-2} were studied in detail and are further referred to as low fluence and high fluence respectively. The samples are 300 to 500 μm thick plates of HPHT-grown type Ib single crystal diamond produced by «AdamasInvest». The plates were cut and polished along (100) crystallographic plane. The concentration of nitrogen impurity in the form of C-defects in yellow and colorless areas of the plates is about 150 ppm and a few ppm, respectively [14]. After the ion implantation, the plates were cross-sectionally cut perpendicular to the implanted surface and along the irradiation direction. The cut surfaces were mechanically polished. These cross-sectional surfaces were used for the studies of the depth distribution of the radiation damage.

Photoluminescence (PL) and Raman scattering of the samples were measured using Raman spectrometer Nanofinder HE (LOTIS TII Japan-Belarus) combined with confocal microscope and 3D sample stage. Spectral and spatial resolutions of the system were 0.25 cm^{-1} and 0.5 μm respectively [15]. Lasers with wavelengths 355, 532 and 785 nm were used for the excitation. PL measurements were performed at liquid nitrogen temperature (LNT). Raman spectra were taken at room temperature (RT). Integral intensities and spectral widths (full width at half magnitude, FWHM) of PL and Raman lines were calculated from the fittings by pseudo-Void function. The peak intensities of PL lines were scaled relative to the intensity of the diamond Raman line.

After the samples were studied in the as-irradiated state, they were annealed in vacuum (residual pressure about 10^{-3} Pa) at a temperature of 1450 °C for 1 h in a graphite container. The times of ramping temperature up and down were about 10 min and 30 min correspondingly. After the annealing, the samples were cleaned in a saturated solution of potassium dichromate in sulfuric acid.

3. Results and discussion

3.1. Raman scattering

Fig. 1a shows the emission spectra taken from the cross-sectional side of the sample irradiated with the high fluence. The high fluence irradiation is sufficient to completely quench luminescence. Therefore all the features shown in the spectra are due to Raman scattering [7]. The narrow line at wavenumber 1332 cm^{-1} is the first order diamond Raman line. The narrow lines in the spectral range 1400–1900 cm^{-1} relate to point radiation defects characteristic of ion-irradiated diamond

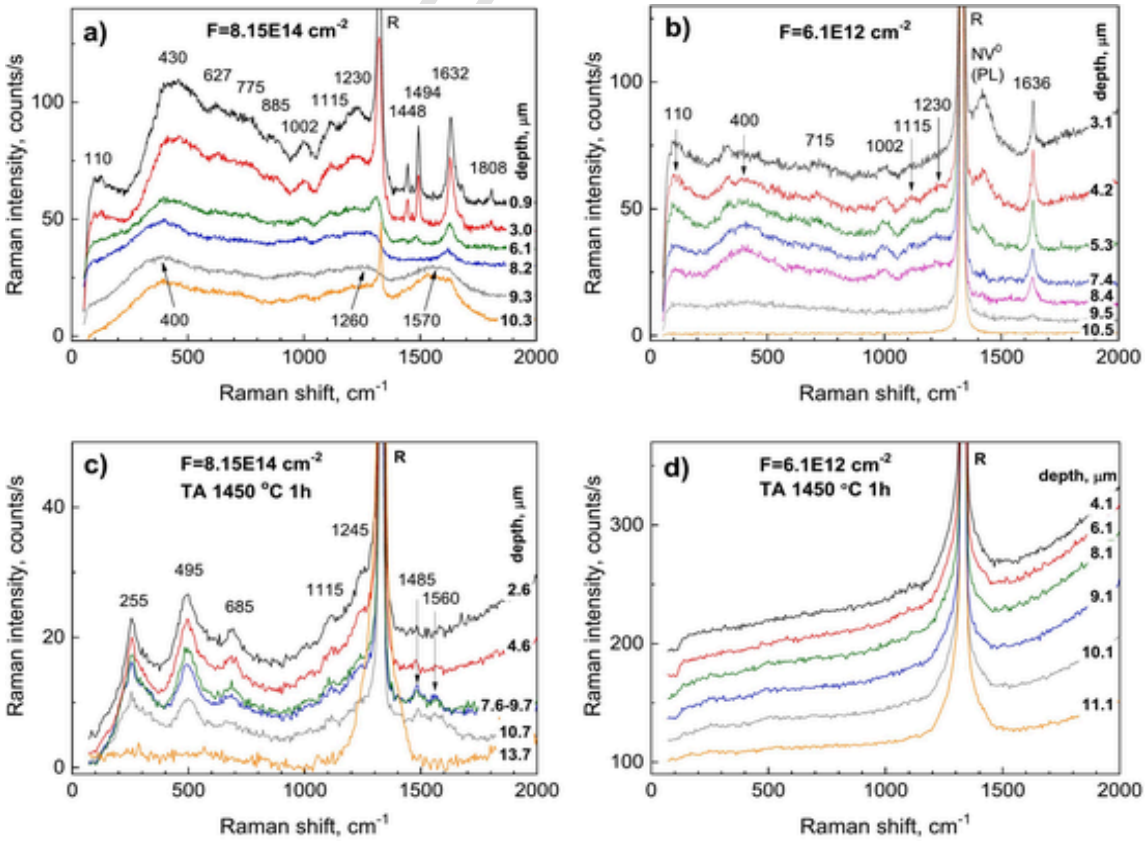

Fig. 1. Raman spectra taken from the cross-sectional side at different distances (from the irradiated surface (shown in micrometers): (a, b) – as-irradiated, excitation with 532 nm laser, high fluence (a) and low fluence (b); (c, d) – after annealing, excitation with 355 nm laser (for PL suppress), high fluence (c) and low fluence (d). All spectra are shown as measured. No vertical shift "for clarity" was done. Sharp signal cut-off at wavenumbers below 100 cm^{-1} is the absorption of the optical filter.

[16]. Of them, the lines at 1494 cm^{-1} and 1632 cm^{-1} are ascribed to vacancies and self-interstitials respectively [12,17,18].

Other Raman features of the as-irradiated sample are observed at wavenumbers 430, 627, 775, 1002, 1115 and 1230 $см^{-1}$. Some of them were observed previously in the Raman spectra of ion-irradiated [1,12,17,19,20], neutron-irradiated diamonds [20–22], and nanodiamonds [23]. Spectral positions of these lines but the broad band at wavenumber 430 cm^{-1} correspond to the maxima of the phonon density of diamond lattice [24–27]. Based on this correspondence and taking into account that all the phonons with the exception of those with wavenumber 1332 cm^{-1} are forbidden in Raman scattering from ideal diamond crystal, a conclusion is made that the spectrum shown in Fig. 1a is a Raman signature of disordered "amorphous diamond" [12,17,22,23].

The Raman signal of "amorphous diamond" is also detected in samples irradiated with the low fluence (Fig. 1b). This observation suggests that the "amorphization" of diamond may occur in every track produced by swift ions, even by light He ions [12,17]. In the present case of heavy Xe ions, this assumption seems to be much more plausible. The process of "amorphization" could be interpreted as the result of very rapid local destruction or "melting" of diamond lattice due to strong release of energy in electronic stopping and subsequent instantaneous freezing. This mechanism is expected to be similar to that described in [28].

The narrow lines at wavenumbers 1448 and 1494 cm^{-1} can be traced to a depth of 6.1 μm, whereas the line at 1632 cm^{-1} is clearly detected through the whole ion irradiated depth. A similar difference in the depth distribution is also observed between the luminescence centers which require thermal activation after irradiation (shallow penetration) and the luminescence centers which form directly during irradiation (deep penetration, see below). Based on this similarity we assume that the defects behind the 1448 and 1494 cm^{-1} Raman lines also require some heating for their formation, whereas elevated temperature is not required for defects behind the 1632 cm^{-1} line. At the depths corresponding to the maximum nuclear stopping power (a layer from about 8 to 10 μm where the diamond Raman line 1332 cm^{-1} is not detected), only broad bands with maxima at 400, 1260 and 1570 cm^{-1} are observed suggesting complete disorder of the diamond crystal lattice. The remnants of the interstitial-related Raman line can be discerned at a wavenumber of 1632 cm^{-1} too.

The band at wavenumber 1570 cm^{-1} appears only in spectra of samples irradiated with high fluences (in our case at fluences over 3.55×10^{14} ions/cm^2 [7]). This band has been reported in a number of publications on diamonds irradiated with ions [12,18,29–34] and neutrons [20–22]. The occurrence of this band has been associated with the critical density of radiation damage at which the diamond structure changes from crystalline to some kind of amorphous carbon which, upon annealing, transforms to graphite [35,36]. The spectral position and shape of the 1570 cm^{-1} band coincided with those from graphite strongly disordered by ion implantation [18,30,31,37,38].

High temperature annealing activated luminescence which was especially strong when excited with green laser. Due to this circumstance the Raman measurements of the annealed samples were performed with 355 nm laser. After the annealing, Raman spectra changed substantially (Fig. 1c-d). The lines 1448 cm^{-1}, 1494 cm^{-1} and 1632 cm^{-1} disappeared. Practically no measurable features related to disordered diamond could be detected in the low fluence sample. The spectrum of the high fluence sample revealed three distinctive bands at wavenumbers 225, 495, 685 cm^{-1} and two minor features at 1115 and 1245 cm^{-1}. Similar Raman features were observed previously after annealing of ion-implanted diamonds [12,22,39]. The Raman bands observed after annealing are noticeably narrower than those in spectra of the as-irradiated samples. This narrowing suggests that the irregular "amorphous" atomic structure transformes during heating into a structurally more ordered one.

After annealing, the Raman spectra of high fluence sample revealed the presence of the diamond Raman line over the whole irradiated volume. However, its intensity at the depth of the ion projected range remains substantially suppressed. The broad band 1570 cm^{-1} disappeared giving way to two weak narrow lines at 1485 cm^{-1} and 1560 cm^{-1} with FWHM about 35–40 cm^{-1} (Fig. 1c). These lines were also observed in spectra of low-quality CVD diamonds [40] and highly deformed diamonds [41]. They were ascribed to some non-diamond carbon clusters. It is well known that shallow diamond layers irradiated with high fluences of low energy ions transform into graphite after annealing performed without stabilizing pressure [18,35,36,42]. In contrast to those observations, no graphitization occurs in deeply buried ion-damaged layers even when the fluence is expected to be sufficient to produce amorphization. A common explanation of the suppression of graphitization in the buried diamond layers is the pressure produced by the adjacent crystalline diamond [18,24,25,35,42–44]. Taking this consideration into account, we assume that the lines at wavenumbers of 1485 cm^{-1} and 1560 cm^{-1}, which appeared after annealing, are not features of the graphitization.

The depth distribution of the intensity, width and spectral position of the diamond Raman line (nominal spectral position at 1332 cm^{-1}) is shown in Fig. 2. The minimum intensity, maximum shift and the maximum broadening of this line manifest the depth of the maximum damage. The increase in the shift and broadening of the diamond Raman line with depth is in a good agreement with the depth distribution of primary vacancies (radiation damage) calculated with SRIM 2000 code [7,11,12,33,45]. The line broadening is the result of increasing nonhomogeneous distortions of the crystal lattice [7,45], whereas the line shift suggests a substantial component of hydrostatic (3D expansion) and/or directional (1D and 2D tensile) stress [1,46–48]. The magnitude of this stress in the maximum damaged layer of the high fluence sample can reach 10 GPa (as estimated using the data from [48]). The decrease in the line intensity with the depth is the result of the increasing opacity and the reduction in the phonon lifetime as the ion damage increases [12,22].

The intensity, width and spectral position of the diamond Raman line have been largely returned to their values measured before irradiation. The tensile stress in the layer of maximum damage produced by the fluence 8.15×10^{14} cm^{-2} is 5 times down to 2 GPa after the annealing. A remarkable observation is a small but well detectable positive shift of the diamond Raman line right after the ion-irradiated layer, at a depth of 10 μm. This positive shift strongly suggests the development of compressive stress at the interface between the ion-damaged layer and the adjacent nominally non-damaged layer.

3.2. PL spectra

PL intensity was drastically suppressed in the whole volume irradiated with fluences over 10^{13} cm^{-2}. Therefore, only the low fluence sample was used for the investigations of the depth distribution of the luminescence active defects. PL was excited with 355 nm and 532 nm lasers in colorless cubic (100) sectors which exhibited relatively weak luminescence of the nickel-related centers [49,50]. The irradiation induced many centers (Fig. 3a), the most prominent of which were the 389 nm, 453 nm, 508 nm, ND1, TR12, 3H, NV^0, NV^- and GR1 centers. Most of them have been well studied before [51–53]. The 389 nm center is ascribed to carbon interstitial trapped by single nitrogen atom. The centers TR12 (ZPL at 470 nm) and 3H (ZPL at 503.5 nm) are attributed to intrinsic defects containing interstitials. The centers ND1 (ZPL at 393 nm) and GR1 (ZPL at 741 nm) are single vacancies in negative and neutral charge states. The NV^0 and NV^- are nitrogen-vacancy defects in neutral and negative charge states.

Qualitatively, PL spectra retain their composition over the whole irradiated layer. The PL intensity of all centers (Fig. 3c) monotonously decreases with depth as the nuclear stopping power and the radiation

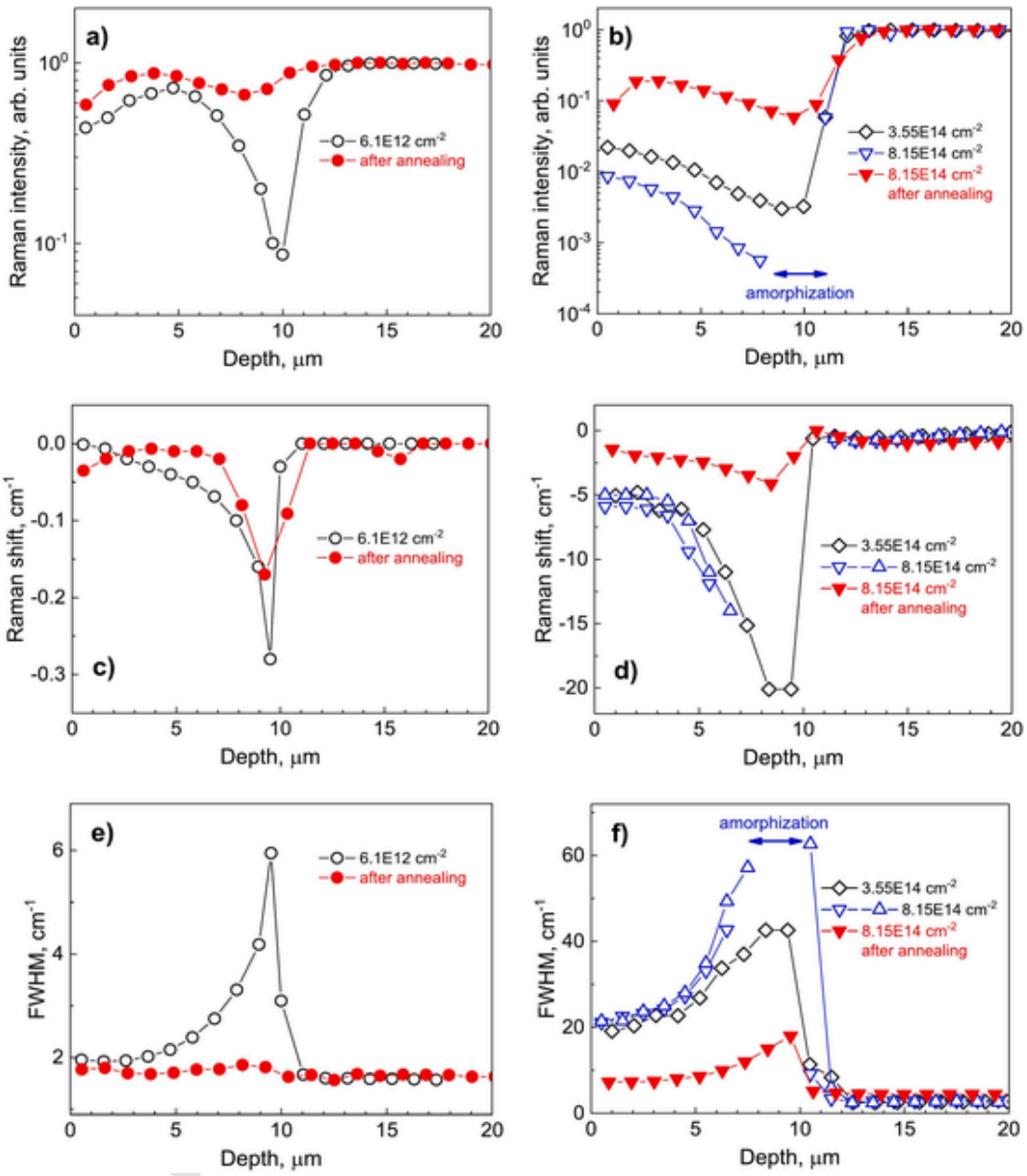

Fig. 2. Depth distribution of the intensity (a, b), spectral position (c, d) and FWHM (e, f) of the diamond Raman line before and after annealing in the low (left graphs) and high (right graphs) fluence.

damage increase [7]. Intensities of the GR1, ND1 and 453 nm centers show some enhanced suppression at depths around 9 μm. This suppression is especially evident for the 389 nm center which actually is undetectably weak at a depth of 9 μm. As the luminescence intensity decreases the spectral width of all ZPLs goes up attaining maximum at the depth of the ion projected range. Comparing the depth distributions of the intensities and spectral widths (Fig. 3e) we deduce that the maximum radiation damage has occurred in a narrow layer at a depth from about 8.5 μm to 9.5 μm. This depth interval well agrees with the deduced from the Raman measurements.

The broadening of ZPLs is qualitatively very different for different centers. Close to the surface, the increase in the line width for the interstitial-type defects TR12 and 3H was in the range of 0.2 to 1.2 meV ("hard" centers), whereas for the vacancy-related centers GR1, ND1, NV^0, NV^- it was much greater ranging from 2.3 to 2.6 meV ("soft" centers). The broadening of the ZPL 508 nm is in the range of the "hard" centers. The ZPL width of the 453 nm center behaves similarly to the "soft" vacancy-related centers. These observations allow us to assume that the 508 nm is a manifestation of an interstitial-type defect, whereas the 453 nm center is rather related to a vacancy-containing defect. The 389 nm center, also being commonly regarded as an interstitial-related one, shows dramatic increase in its ZPL width which even surpasses the broadening of the "softest" vacancy-related centers. This very "soft" behavior of the 389 nm center may raise some concern about its atomic model.

It is to note that the optical centers related to the intrinsic radiation defects containing interstitials (TR12, 3H, 508 nm) and NV defects are not detected beyond the layer of the maximum damage. In contrast, the vacancy-related GR1, ND1 and 453 nm centers as well as the nitrogen-related, interstitial-related 389 nm center penetrate beyond the maximum damage layer reaching through the whole ion-irradiated depth.

The depth distribution of intensity of the discussed optical centers in the irradiated layer can be qualitatively described by the distribution of the nuclear stopping power which is the major mechanism of the radia-

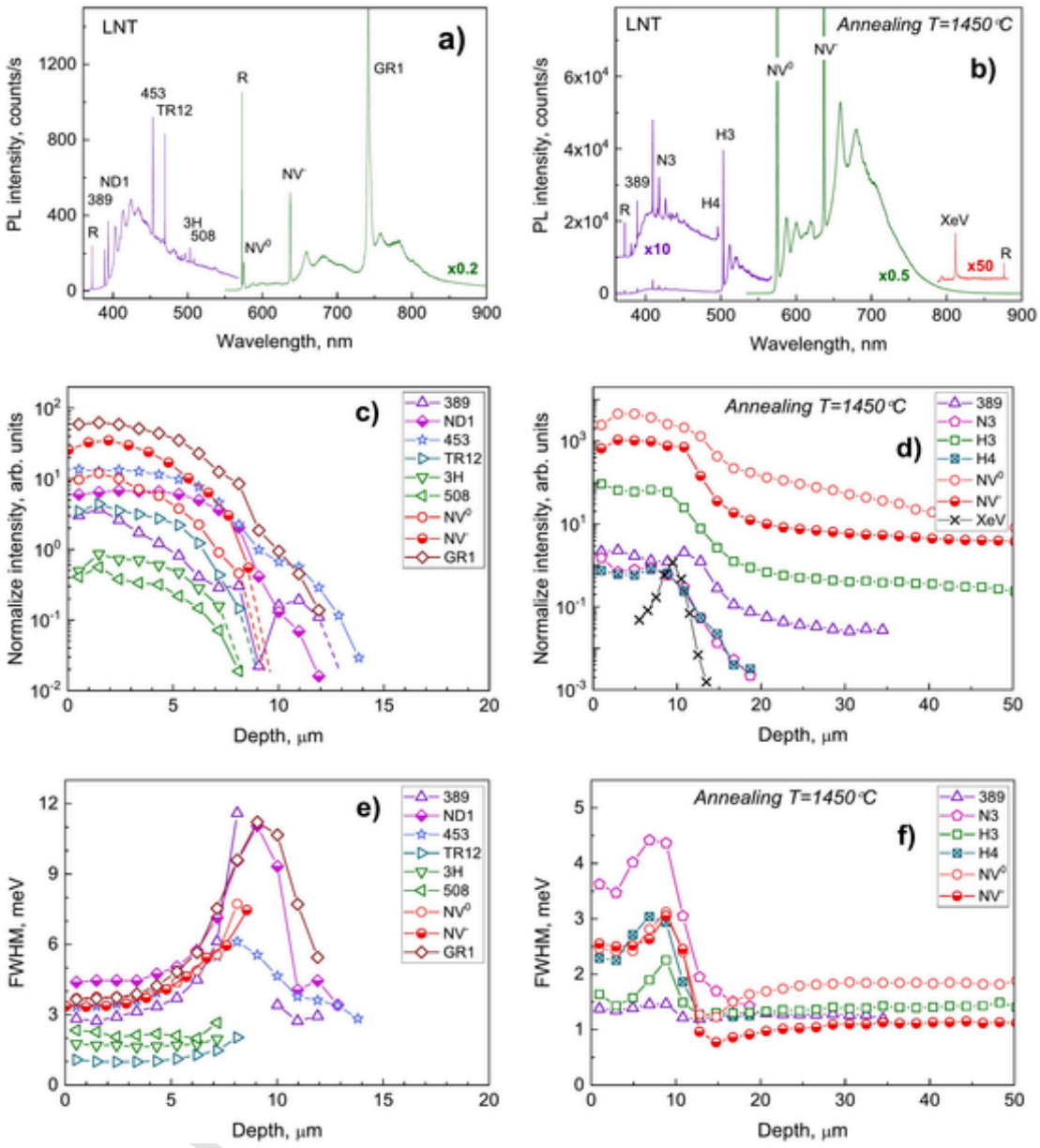

Fig. 3. Representative PL spectra (a, b) and distribution of intensity (c, d) and line width (e, f) along the depth in the low fluence sample before (left graphs) and after (right graphs) annealing. Lasers with wavelengths 355, 532 and 785 nm were used for PL excitation.

tion damage in ion-implanted diamond. In luminescence, the radiation damage reveals itself in two opposite ways. On one hand, it increases the concentration of radiation defects. On the other hand, radiation damage strongly quenches the luminescence efficiency via increasing the intensity of non-radiative mechanisms of relaxation and recombination. For the ion fluences used in this research, the luminescence quenching is a dominating effect [7]. Therefore, the luminescence intensity of all centers in the as-irradiated samples decreases with depth as the nuclear stopping power increases.

An interesting feature of the PL spectra taken from as-irradiated samples is the rather intense NV centers, which have formed directly during irradiation. Our previous studies on NV centers have shown that the probability of their direct formation during electron and low energy ion implantation is low [52]. PL activation of NV centers requires post irradiation annealing at temperatures over 500 °C [54]. This "irradiation-plus-annealing" process is commonly interpreted as the formation of vacancies during irradiation and the diffusion of vacancies and their capture by nitrogen during annealing. The defects formation of which requires post-irradiation annealing are usually referred to as secondary radiation defects. NV defects are typical secondary radiation defects. However, during high energy ion irradiation NV defects form directly during irradiation. This fact strongly suggests that high energy ions produce instantaneous local heating during their stopping. Since the depth distribution of NV centers resembles that of the electronic stopping of Xe ions of energy 1 MeV/amu (maximum at the surface and low at the depth of the ion penetration), we assume that the electronic stopping is the major source of the heating. We estimate that this heating is equivalent to the stationary annealing at temperatures from 600 to 700 °C. The upper temperature limit of 700 °C follows from the fact that all the primary radiation centers of low temperature stability (3H, TR12, GR1, ND1) which anneal out at temperatures over 700 °C remain intense in PL spectra of as-irradiated samples.

After annealing, all intrinsic radiation centers disappear and the dominating features are the centers NV^0, NV^- and H3 (Fig. 3d). The

other minor centers are 389 nm, N3, and H4. These centers represent different stages of the nitrogen aggregation: single nitrogen atoms (centers 389 nm, NV^0, NV^-), two nitrogen atoms (center H3), three nitrogen atoms (center N3) and four nitrogen atoms (center H4) [52,53]. The location of the ion-implanted layer can be well traced by the presence of the Xe-related optical center with ZPL at 794 and 811 nm (Xe atom bound to vacancy, Xe—V defect) [3,55,56], which is activated by annealing. The luminescence of Xe—V defects can be detected at depths from 5 to 13 μm with maximum intensity at 9.5 μm. This value is approximately 1 μm less than the calculated with SRIM 2000 code [57]. The intensity of all nitrogen-related centers remains relatively constant at depths up to the ion-implanted layer. Beyond the ion-implanted layer the luminescence intensity gradually decreases yet remains of a considerable magnitude far beyond the ion-implanted layer.

After annealing, the spectral widths of ZPLs of nitrogen-related centers increase with depth and then sharply drop when passing the ion-implanted layer (Fig. 3f). Right beyond the ion-implanted layer, the ZPL widths show a distinctive minimum and, at greater depths, the ZPL widths gradually restore to their values observed in non-irradiated samples.

Although the widths of all ZPLs are strongly reduced after annealing, they do not come to their normal values observed in non-irradiated samples. A peculiar feature is the maximum reduction of the line widths observed at depths from 15 to 18 μm. The widths returned to their normal values only at depths over 30 μm. A preliminary explanation of this strange narrowing may suggest the formation of some unstressed micro areas behind the ion-implanted layer.

It is very remarkable that after the annealing, all nitrogen-related centers NV, H3, N3, H4, and 389 nm reveal substantial presence at depths far beyond the ion-implanted layer, actually through the whole thickness of the sample. This deep penetration of typical radiation defects is the manifestation of the crystal lattice damage occurring far beyond the area of the direct radiation damaged produced by ions. The diffusion of vacancies and interstitials from the ion-irradiated layer cannot explain this effect. Indeed, the distances are too long, the diffusion coefficients are too small, and the annealing temperature and time are insufficient for any measurable diffusion length. The only plausible explanation seems to be the mechanical deformation spreading from the highly stressed layer of maximum damage. The magnitude of this stress can be evaluated from the broadening and the shift of the Raman line and ZPLs of optical centers. We found that it can be in the range of a few GPa. The post-implantation annealing facilitates plastic deformation [58,59] and, consequently, reduces stress via the generation of dislocations [60]. The stress relaxation is evidenced by the reduction of broadening and shift of all spectral lines. Dislocations, while being created and while moving, generate vacancies and interstitials [61,62]. In turn, the vacancies and interstitials are captured by single nitrogen atoms and form NV and 389 nm centers. Besides, the vacancies stimulate nitrogen aggregation promoting the formation of H3, H4 and N3 centers [63,64]. The proposed formation of vacancies during the relaxation of the stressed area behind the ion-implanted layer appears to be no small effect. The concentration of vacancies is high enough not only to create high concentration of NV defects, but also to facilitate the nitrogen aggregation and formation of H3, N3 and H4 defects.

4. Conclusion

Raman and photoluminescence spectroscopy has been used to study the depth distribution of the radiation-induces damage produced by Xe ions of energy 167 MeV in diamond after irradiation and after subsequent annealing at a temperature of 1450 °C. Low ion fluences below the amorphization threshold and high fluences above the amorphization threshold have been studied. It is found that the ion irradiation forms three distinctive layers characterized by specific defect structure.

The first layer (the high energy layer) spreads from the surface to the depth of the maximum nuclear stopping power. This layer is formed directly during the ion irradiation. The characteristic of this layer is the presence of the primary (centers ND1, GR1, TR12, 3H, 389 nm) and secondary (centers NV^0 and NV^-) radiation defects right after irradiation. The primary radiation defects are the result of the nuclear stopping occurring via atomic collisions. The secondary radiation defects are formed by simultaneous action of the atomic collisions and local heating due to strong electronic stopping. The manifestation of the secondary radiation defects is the centers NV^0 and NV^-. In the case of 167 MeV Xe ions, the effect of the heating instantaneously generated in the high energy layer is equivalent to the effect of stationary annealing at a temperature of 600–700 °C.

The second layer (the maximum damage layer) is formed behind the high energy layer at the depth of the maximum nuclear stopping power. This layer essentially coincided with the ion-implanted layer. The defect structure of the maximum damage layer forms directly during irradiation. If the ion irradiation is performed with high fluences, diamond in the maximum damage layer may completely lose its crystalline structure and can be regarded as amorphous diamond. This amorphization is detected as the disappearance of the Raman features of crystalline diamond. For 167 MeV Xe ions the amorphous diamond layer may formed at fluences above 3×10^{14} cm^{-2}.

The third layer (the layer behind the maximum damage layer, distant layer) may spread many times the ion penetration depth. We assume that the defect structure of this layer is formed by the dislocations propagating from the maximum damage layer into the diamond bulk and by the point defects generated during the motion of dislocations. These point defects are the secondary radiation defects NV^0, NV^-, H3, N3 and 389 nm center. Since primary radiation defects do not form in the distant layer, the presence of this layer can be detected in luminescence after post-irradiation annealing at temperatures over 700 °C.

Annealing at a temperature of 1450 °C does not fully restore the crystal lattice in the irradiated layer. Substantial concentration of defects is evidenced by the presence of Raman bands at 225, 495, 685, 1115, и 1245 cm^{-1} in the spectra of the high energy layer and by the band at 1485 cm^{-1} и 1560 cm^{-1} in the spectra of the maximum damage layer.

CRediT authorship contribution statement

N.M. Kazuchits: Writing – original draft, Supervision, Project administration, Investigation, Funding acquisition, Formal analysis, Conceptualization. **V.N. Kazuchits:** Visualization, Investigation, Formal analysis. **O.V. Korolik:** Investigation. **M.S. Rusetsky:** Software, Investigation. **V.A. Skuratov:** Resources, Investigation. **A.M. Zaitsev:** Writing – original draft, Formal analysis, Conceptualization.

Author agreement statement

We the undersigned declare that this manuscript is original, has not been published before and is not currently being considered for publication elsewhere.

We confirm that the manuscript has been read and approved by all named authors and that there are no other persons who satisfied the criteria for authorship but are not listed. We further confirm that the order of authors listed in the manuscript has been approved by all of us.

We understand that the Corresponding Author is the sole contact for the Editorial process. He/she is responsible for communicating with the other authors about progress, submissions of revisions and final approval of proofs.

Declaration of competing interest

The authors declare that they have no known competing financial interests or personal relationships that could have appeared to influence the work reported in this paper.

Acknowledgements

N.M.K., V.N.K. and M.S.R. acknowledge the State Research Program "Materials science, new materials and technologies" of the Republic of Belarus [grant number 1.6.3] for financial support.

Data availability

Data will be made available on request.

References

[1] S. Prawer, R.J. Nemanich, Raman spectroscopy of diamond and doped diamond, Philos. Trans. R. Soc. A Math. Phys. Eng. Sci. 362 (2004) 2537–2565, https://doi.org/10.1098/rsta.2004.1451.
[2] A.C. Ferrari, Raman spectroscopy of graphene and graphite: disorder, electron-phonon coupling, doping and nonadiabatic effects, Solid State Commun. 143 (2007) 47–57, https://doi.org/10.1016/j.ssc.2007.03.052.
[3] A.M. Zaitsev, High energy ion implantation into diamond and cubic boron nitride, Nucl. Instruments Methods Phys. Res. Sect. B Beam Interact. Mater. Atoms 62 (1991) 81–98, https://doi.org/10.1016/0168-583X(91)95933-5.
[4] M. Toulemonde, C. Dufour, E. Paumier, Transient thermal process after a high-energy heavy-ion irradiation of amorphous metals and semiconductors, Phys. Rev. B 46 (1992) 14362–14369, https://doi.org/10.1103/PhysRevB.46.14362.
[5] S. Eaton-Magaña, C.M. Breeding, R. Bassoo, Low-temperature annealing and kinetics of radiation stains in natural diamond, Diamond Relat. Mater. 132 (2023) 109649, https://doi.org/10.1016/j.diamond.2022.109649.
[6] K. Wang, J. Steeds, Z. Li, Photoluminescence studies of 515.8nm, 533.5nm and 580nm centres in electron irradiated type IIa diamond, Diamond Relat. Mater. 25 (2012) 29–33, https://doi.org/10.1016/j.diamond.2012.02.012.
[7] N.M. Kazuchits, O.V. Korolik, M.S. Rusetsky, V.N. Kazuchits, N.S. Kirilkin, V.A. Skuratov, Raman scattering in diamond irradiated with high-energy xenon ions, Nucl. Instruments Methods Phys. Res. Sect. B Beam Interact. Mater. Atoms 472 (2020) 19–23, https://doi.org/10.1016/j.nimb.2020.03.034.
[8] G. García, M. Díaz-Híjar, V. Tormo-Márquez, I. Preda, O. Peña-Rodríguez, J. Olivares, Structural damage on single-crystal diamond by swift heavy ion irradiation, Diamond Relat. Mater. 58 (2015) 226–229, https://doi.org/10.1016/j.diamond.2015.08.014.
[9] J.F. Prins, T.E. Derry, J.P.F. Sellschop, Volume expansion of diamond during ion implantation, Phys. Rev. B 34 (1986) 8870–8874, https://doi.org/10.1103/PhysRevB.34.8870.
[10] J.F. Prins, T.E. Derry, J.P.F. Sellschop, Volume expansion of diamond during ion implantation at low temperatures, Nucl. Instruments Methods Phys. Res. Sect. B Beam Interact. Mater. Atoms 18 (1986) 261–263, https://doi.org/10.1016/S0168-583X(86)80041-6.
[11] D.N. Jamieson, S. Prawer, K.W. Nugent, S.P. Dooley, Cross-sectional Raman microscopy of MeV implanted diamond, Nucl. Instruments Methods Phys. Res. Sect. B Beam Interact. Mater. Atoms 106 (1995) 641–645, https://doi.org/10.1016/0168-583X(96)80036-X.
[12] J.O. Orwa, K.W. Nugent, D.N. Jamieson, S. Prawer, Raman investigation of damage caused by deep ion implantation in diamond, Phys. Rev. B - Condens. Matter Mater. Phys. 62 (2000) 5461–5472, https://doi.org/10.1103/PhysRevB.62.5461.
[13] F.F. Komarov, Defect and track formation in solids irradiated by superhigh-energy ions, Physics-Uspekhi 46 (2003) 1253–1282, https://doi.org/10.1070/PU2003v046n12ABEH001286.
[14] N.M. Kazuchits, M.S. Rusetsky, V.N. Kazuchits, O.V. Korolik, V. Kumar, K.S. Moe, W. Wang, A.M. Zaitsev, Comparison of HPHT and LPHT annealing of Ib synthetic diamond, Diamond Relat. Mater. 91 (2019) 156–164, https://doi.org/10.1016/j.diamond.2018.11.018.
[15] I. Kudryashov, P. Rutkovski, S. Suruga, Advanced 3-D Confocal Microscope for Raman Imaging Spectroscopy, Tokyo Instruments, Inc., 2002.
[16] J.D. Hunn, S.P. Withrow, C.W. White, D.M. Hembree, Raman scattering from MeV-ion implanted diamond, Phys. Rev. B 52 (1995) 8106–8111, https://doi.org/10.1103/PhysRevB.52.8106.
[17] S. Prawer, K.W. Nugent, D.N. Jamieson, The Raman spectrum of amorphous diamond, Diamond Relat. Mater. 7 (1998) 106–110, https://doi.org/10.1016/S0925-9635(97)00194-5.
[18] R. Kalish, A. Reznik, S. Prawer, D. Saada, J. Adler, Ion-implantation-induced defects in diamond and their annealing: experiment and simulation, Phys. Status Solidi 174 (1999) 83–99, https://doi.org/10.1002/(SICI)1521-396X(199907)174:1<83::AID-PSSA83>3.0.CO;2-3.
[19] O.N. Poklonskaya, A.A. Khomich, Raman scattering in a diamond crystal implanted by high-energy nickel ions, J. Appl. Spectrosc. 80 (2013) 715–720, https://doi.org/10.1007/s10812-013-9831-3.
[20] O.N. Poklonskaya, S.A. Vyrko, A.A. Khomich, A.A. Averin, A.V. Khomich, R.A. Khmelnitsky, N.A. Poklonskia, Raman scattering in natural diamond crystals implanted with high-energy ions and irradiated with fast neutrons, J. Appl. Spectrosc. 81 (2015) 969–977, https://doi.org/10.1007/s10812-015-0037-8.
[21] A.V. Khomich, R.A. Khmelnitskii, X.J. Hu, A.A. Khomich, A.F. Popovich, I.I. Vlasov, V.A. Dravin, Y.G. Chen, A.E. Karkin, V.G. Ralchenko, Radiation damage effects on optical, electrical, and thermophysical properties of cvd diamond films, J. Appl. Spectrosc. 80 (2013) 707–714, https://doi.org/10.1007/s10812-013-9830-4.
[22] A.A. Khomich, R.A. Khmelnitsky, A.V. Khomich, Probing the nanostructure of neutron-irradiated diamond using raman spectroscopy, Nanomaterials 10 (2020) 1166, https://doi.org/10.3390/nano10061166.
[23] S. Prawer, K.W. Nugent, D.N. Jamieson, J.O. Orwa, L.A. Bursill, J.L. Peng, The Raman spectrum of nanocrystalline diamond, Chem. Phys. Lett. 332 (2000) 93–97, https://doi.org/10.1016/S0009-2614(00)01236-7.
[24] P. Pavone, K. Karch, O. Schütt, D. Strauch, W. Windl, P. Giannozzi, S. Baroni, Ab initio lattice dynamics of diamond, Phys. Rev. B 48 (1993) 3156–3163, https://doi.org/10.1103/PhysRevB.48.3156.
[25] W. Windl, P. Pavone, K. Karch, O. Schütt, D. Strauch, P. Giannozzi, S. Baroni, Second-order Raman spectra of diamond from ab initio phonon calculations, Phys. Rev. B 48 (1993) 3164–3170, https://doi.org/10.1103/PhysRevB.48.3164.
[26] C.Z. Wang, K.M. Ho, Structure, dynamics, and electronic properties of diamondlike amorphous carbon, Phys. Rev. Lett. 71 (1993) 1184–1187, https://doi.org/10.1103/PhysRevLett.71.1184.
[27] A. Bosak, M. Krisch, Phonon density of states probed by inelastic x-ray scattering, Phys. Rev. B - Condens. Matter Mater. Phys. 72 (2005) 1–9, https://doi.org/10.1103/PhysRevB.72.224305.
[28] Z. Zeng, L. Yang, Q. Zeng, H. Lou, H. Sheng, J. Wen, D.J. Miller, Y. Meng, W. Yang, W.L. Mao, H. Mao, Synthesis of quenchable amorphous diamond, Nat. Commun. 8 (2017) 322, https://doi.org/10.1038/s41467-017-00395-w.
[29] E.H. Lee, D.M. Hembree, G.R. Rao, L.K. Mansur, Raman scattering from ion-implanted diamond, graphite, and polymers, Phys. Rev. B 48 (1993) 15540–15551, https://doi.org/10.1103/PhysRevB.48.15540.
[30] R. Brunetto, G.A. Baratta, G. Strazzulla, Raman spectroscopy of ion irradiated diamond, J. Appl. Phys. 96 (2004) 380–386, https://doi.org/10.1063/1.1759080.
[31] R. Brunetto, G.A. Baratta, G. Strazzulla, Amorphization of diamond by ion irradiation: a Raman study, J. Phys. Conf. Ser. 6 (2005) 120–125, https://doi.org/10.1088/1742-6596/6/1/011.
[32] H. Amekura, N. Kishimoto, Effects of high-fluence ion implantation on colorless diamond self-standing films, J. Appl. Phys. 104 (2008), https://doi.org/10.1063/1.2978215.
[33] R.A. Khmelnitsky, V.A. Dravin, A.A. Tal, E.V. Zavedeev, A.A. Khomich, A.V. Khomich, A.A. Alekseev, S.A. Terentiev, Damage accumulation in diamond during ion implantation, J. Mater. Res. 30 (2015) 1583–1592, https://doi.org/10.1557/jmr.2015.21.
[34] A. Deslandes, M.C. Guenette, C.S. Corr, I. Karatchevtseva, L. Thomsen, G.R. Lumpkin, D.P. Riley, Deuterium retention and near-surface modification of ion-irradiated diamond exposed to fusion-relevant plasma, Nucl. Fusion 54 (2014) 073003, https://doi.org/10.1088/0029-5515/54/7/073003.
[35] C. Uzan-Saguy, C. Cytermann, R. Brener, V. Richter, M. Shaanan, R. Kalish, Damage threshold for ion-beam induced graphitization of diamond, Appl. Phys. Lett. 67 (1995) 1194–1196, https://doi.org/10.1063/1.115004.
[36] R. Kalish, S. Prawer, Graphitization of diamond by ion impact: fundamentals and applications, Nucl. Inst. Methods Phys. Res. B 106 (1995) 492–499, https://doi.org/10.1016/0168-583X(95)00758-X.
[37] G. Strazzulla, G.A. Baratta, F. Spinella, Production and evolution of carbonaceous material by ion irradiation in space, Adv. Sp. Res. 15 (1995) 385–399, https://doi.org/10.1016/S0273-1177(99)80109-4.
[38] G.A. Baratta, V. Mennelia, J.R. Brucato, L. Colangeli, G. Leto, M.E. Palumbo, G. Strazzulla, Raman spectroscopy of ion-irradiated interplanetary carbon dust analogues, J. Raman Spectrosc. 35 (2004) 487–496, https://doi.org/10.1002/jrs.1169.
[39] F. Agulló-Rueda, M.D. Ynsa, N. Gordillo, A. Maira, D. Moreno-Cerrada, M.A. Ramos, Micro-Raman spectroscopy of near-surface damage in diamond irradiated with 9-MeV boron ions, Diamond Relat. Mater. 72 (2017) 94–98, https://doi.org/10.1016/j.diamond.2017.01.010.
[40] B. Zhang, S. Chen, Morphological evolution of diamonds in combustion synthesis, J. Appl. Phys. 79 (1996) 7241–7247, https://doi.org/10.1063/1.361441.
[41] Y.G. Gogotsi, A. Kailer, K.G. Nickel, Pressure-induced phase transformations in diamond, J. Appl. Phys. 84 (1998) 1299–1304, https://doi.org/10.1063/1.368198.
[42] R. Kalish, A. Reznik, K.W. Nugent, S. Prawer, The nature of damage in ion-implanted and annealed diamond, Nucl. Instruments Methods Phys. Res. Sect. B Beam Interact. Mater. Atoms 148 (1999) 626–633, https://doi.org/10.1016/S0168-583X(98)00857-X.
[43] F. Agulló-Rueda, N. Gordillo, M.D. Ynsa, A. Maira, J. Cañas, M.A. Ramos, Lattice damage in 9-MeV-carbon irradiated diamond and its recovery after annealing, Carbon N. Y. 123 (2017) 334–343, https://doi.org/10.1016/j.carbon.2017.07.076.
[44] P. Aprà, J. Ripoll-Sau, J. Manzano-Santamaría, C. Munuera, J. Forneris, S. Ditalia Tchernij, P. Olivero, F. Picollo, E. Vittone, M.D. Ynsa, Structural characterization of 8 MeV 11B implanted diamond, Diamond Relat. Mater. 104 (2020) 107770, https://doi.org/10.1016/j.diamond.2020.107770.
[45] L. Nasdala, D. Grambole, M. Wildner, A.M. Gigler, T. Hainschwang, A.M. Zaitsev, J.W. Harris, J. Milledge, D.J. Schulze, W. Hofmeister, W.A. Balmer, Radio-colouration of diamond: a spectroscopic study, Contrib. Mineral. Petrol. 165 (2013)

843–861, https://doi.org/10.1007/s00410-012-0838-1.
[46] M.H. Grimsditch, E. Anastassakis, M. Cardona, Effect of uniaxial stress on the zone-center optical phonon of diamond, Phys. Rev. B 18 (1978) 901–904, https://doi.org/10.1103/PhysRevB.18.901.
[47] J.W. Ager, M.D. Drory, Quantitative measurement of residual biaxial stress by Raman spectroscopy in diamond grown on a Ti alloy by chemical vapor deposition, Phys. Rev. B 48 (1993) 2601–2607, https://doi.org/10.1103/PhysRevB.48.2601.
[48] F. Ahmed, K. Durst, S. Rosiwal, J. Fandrey, J. Schaufler, M. Göken, In-situ tensile testing of crystalline diamond coatings using Raman spectroscopy, Surf. Coatings Technol. 204 (2009) 1022–1025, https://doi.org/10.1016/j.surfcoat.2009.04.030.
[49] Y.V. Babich, B.N. Feigelson, A.I. Chepurov, Distribution of H1a-centers in as-grown diamonds of Fe-Ni-C system: FTIR-mapping study, Diamond Relat. Mater. 69 (2016) 8–12, https://doi.org/10.1016/j.diamond.2016.07.001.
[50] A. Yelisseyev, Y. Babich, V. Nadolinny, D. Fisher, B. Feigelson, Spectrospic study of HPHT synthetic diamonds, as grown at 1500°C, Diamond Relat. Mater. 11 (2002) 22–37, https://doi.org/10.1016/S0925-9635(01)00526-X.
[51] N.M. Kazuchits, V.N. Kazuchits, M.S. Rusetsky, A.V. Mazanik, V.A. Skuratov, K.S. Moe, A.M. Zaitsev, Luminescence of negatively charged single vacancies in diamond: ND1 center, Diamond Relat. Mater. 121 (2022) 108741, https://doi.org/10.1016/j.diamond.2021.108741.
[52] A.M. Zaitsev, Optical Properties of Diamond, Springer Berlin Heidelberg, Berlin, Heidelberg, 2001, https://doi.org/10.1007/978-3-662-04548-0.
[53] I.A. Dobrinets, V.G. Vins, A.M. Zaitsev, HPHT-Treated Diamonds, Springer Berlin Heidelberg, Berlin, Heidelberg, 2013, https://doi.org/10.1007/978-3-642-37490-6.
[54] Y. Nisida, Y. Mita, K. Mori, S. Okuda, S. Sato, S. Yazu, M. Nakagawa, M. Okada, Color centers in annealing of neutron-irradiated type Ib and Ia diamonds, in: Mater. Sci. Forum, Switzerland, 1989, pp. 561–566, https://doi.org/10.4028/www.scientific.net/MSF.38-41.561.
[55] V.A. Martinovich, A.V. Turukhin, A.M. Zaitsev, A.A. Gorokhovsky, Photoluminescence spectra of xenon implanted natural diamonds, JOL 102–103 (2003) 785–790, https://doi.org/10.1016/S0022-2313(02)00642-7.
[56] R. Sandstrom, L. Ke, A. Martin, Z. Wang, M. Kianinia, B. Green, W. bo Gao, I. Aharonovich, Optical properties of implanted Xe color centers in diamond, Opt. Commun. 411 (2018) 182–186, https://doi.org/10.1016/j.optcom.2017.11.064.
[57] J. Ziegler, Srim & trim, (n.d.). http://www.srim.org/ (accessed November 15, 2019).
[58] C.A. Brookes, V.R. Howes, A.R. Parry, Multiple slip in diamond due to a nominal contact pressure of 10 GPa at 1,000 °C, Nature 332 (1988) 139–141, https://doi.org/10.1038/332139a0.
[59] D.J. Weidner, Y. Wang, M.T. Vaughan, Strength of diamond, Science (80-.) 266 (1994) 419–422, https://doi.org/10.1126/science.266.5184.419.
[60] E.J. Brookes, J.D. Comins, R.D. Daniel, R.M. Erasmus, A study of plastic deformation profiles of impressions in diamond, Diamond Relat. Mater. 9 (2000) 1115–1119, https://doi.org/10.1016/S0925-9635(99)00203-4.
[61] T. Evans, S.T. Davey, S.H. Robertson, Photoluminescence studies of sintered diamond compacts, J. Mater. Sci. 19 (1984) 2405–2414, https://doi.org/10.1007/BF01058119.
[62] E. Gaillou, J. Post, N.D. Bassim, A.M. Zaitsev, T. Rose, M.D. Fries, R.M. Stroud, A. Steele, J.E. Butler, Spectroscopic and microscopic characterizations of color lamellae in natural pink diamonds, Diamond Relat. Mater. 19 (2010) 1207–1220, https://doi.org/10.1016/j.diamond.2010.06.015.
[63] A.T. Collins, Vacancy enhanced aggregation of nitrogen in diamond, J. Phys. C Solid State Phys. 13 (1980) 2641–2650, https://doi.org/10.1088/0022-3719/13/14/006.
[64] R. Jones, J.P. Goss, H. Pinto, D.W. Palmer, Diffusion of nitrogen in diamond and the formation of A-centres, Diamond Relat. Mater. 53 (2015) 35–39, https://doi.org/10.1016/j.diamond.2015.01.002.